Degenerate four-wave mixing in equilibrium argon arc plasma



1997 J. Phys. D: Appl. Phys. 30 3346

(http://iopscience.iop.org/0022-3727/30/24/013)

J. Phys. D: Appl. Phys. **30** (1997) 3346–3352. Printed in the UK PII: S0022-3727(97)84206-4

# Degenerate four-wave mixing in equilibrium argon arc plasma

**K Musioł†, K Dzierżęga†, E Pawelec†, B Pokrzywka‡, S Pellerin§ and S Łabuz†**

† Institute of Physics, Jagellonian University, ulica Reymonta 4, 30-059 Kraków, Poland
‡ Institute of Physics, Krakow Paedagogical University, ulica Podchorążych 2, 30-084 Kraków, Poland
§ GREMI, Université d'Orléans, BP 6759, 45067 Orléans Cedex 2, France

Received 14 May 1997

**Abstract.** The non-intrusive degenerate four-wave mixing (DFWM) method was used to study the local thermal equilibrium atmospheric-pressure argon arc plasma. The laser wavelength was in resonance with the $4s[3/2]^0$–$4p'[1/2]$ ArI transition, corresponding to the 696.5 nm emission line. The Abrams–Lind theory was verified and proved to be valid under the conditions of our plasma. In the high-laser-intensity limit, the DFWM signals were shown to be exclusively dependent on the population difference between the relevant argon states. Well resolved axial and radial profiles of the plasma temperature and the electron density were determined.

## 1. Introduction

Optical emission spectroscopy (OES) has commonly been used as a basic tool in laboratory plasma investigations. A simple experimental set-up and non-intrusive measurement are its major advantages. The OES proved to be especially useful for probing homogeneous and stable plasmas. However, it becomes less practical when one deals with non-symmetrical and non-uniform media, due to the line-of-sight measurement of an overall plasma luminosity. In the case of an arc plasma, for side-on observation of the plasma column, perfect axial symmetry is assumed and the Abel inversion procedure is required to determine the radial distribution of the emission coefficient. Therefore, due to the prior assumption about the plasma's axial symmetry, information on any plasma asymmetries is lost. The usefulness of the OES method sometimes can be questionable when one is investigating the vicinity of discharge electrodes, where steep gradients of the plasma parameters exist and the symmetry strongly depends on the position of the cathode spot on the electrode surface.

Some laser-based diagnostic techniques offer significant advantages over OES. They permit high spatial and temporal resolution as well as the detection of species that are not emitting. One such technique is the degenerate four-wave mixing (DFWM) method which gives coherent, phase-conjugated and collimated signals that can be readily discriminated against a high plasma luminosity (which is a common difficulty for laser-induced fluorescence methods in bright plasma sources). This technique was used, for the first time, to detect atomic species in a flame seeded with sodium [1]. Since then DFWM has been applied to detect various molecular species such as NO [2], OH [3], CH [4], $C_2$ [5] and $NH_3$ [6] and for determination of their temperature and spatial density distributions.

In this work DFWM, in the phase-conjugate geometry, is applied to study an electric argon arc plasma. The Abrams–Lind theory is briefly described with emphasis on its application for our case of an arc plasma. A norm population difference is introduced in order to derive the plasma temperature from the DFWM signals.

## 2. A description of DFWM

DFWM is a third-order nonlinear optical process in which three laser beams of the same frequency $\omega$ interact with a nonlinear medium to generate a coherent signal beam at the same frequency. A schematic diagram of a DFWM configuration is depicted in figure 1. Two pump beams with electric vectors $\boldsymbol{E}_f$ (forwards) and $\boldsymbol{E}_b$ (backwards) are co-axial and counter-propagating. The third beam $\boldsymbol{E}_p$ (the probe beam) crosses the pump beams' axis at an angle $\theta$. All three beams couple through interaction with the nonlinear medium to generate the fourth beam $\boldsymbol{E}_s$ (the signal) that propagates exactly opposite to and collinear with $\boldsymbol{E}_p$. This geometry satisfies the phase-matching condition for all angles $\theta$. A qualitative description of the DFWM involves interference of all laser beams because they are coherent and oscillate at the same frequency. For instance, the probe beam interferes with the forwards beam, forming a spatial light-intensity modulation pattern with the fringe spacing $\Lambda$ (figure 1(b)),

$$\Lambda = \lambda/[2\sin(\theta/2)] \tag{1}$$

0022-3727/97/243346+07$19.50 

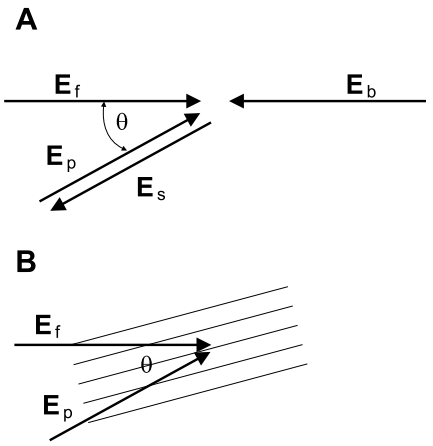


**Figure 1.** (a) A diagram of the DFWM geometry. (b) A schematic drawing of the grating formed by the interference of the forwards and probe laser beams.

where $\lambda$ is the laser wavelength. The spatial oscillation of the light intensity results in a similar variation of the concentration of the upper and lower states of the optical transition. This, in turn, makes the reflection and absorption coefficients vary and thus forms the Bragg grating. The diffraction gratings produced by the interference of $\boldsymbol{E}_p$ with $\boldsymbol{E}_f$ and $\boldsymbol{E}_p$ with $\boldsymbol{E}_b$ result in scattering of $\boldsymbol{E}_b$ and $\boldsymbol{E}_f$, respectively, and generation of the signal beam $\boldsymbol{E}_s$:

$$\boldsymbol{E}_s = \chi(\boldsymbol{E})[(\boldsymbol{E}_f \cdot E_p^*)\boldsymbol{E}_b + (\boldsymbol{E}_b \cdot \boldsymbol{E}_p^*)\boldsymbol{E}_f] \qquad (2)$$

where $\chi(\boldsymbol{E})$ denotes the third-order intensity dependent susceptibility. It can be seen in (2) that $\boldsymbol{E}_s$ is conjugated to $\boldsymbol{E}_p$ which illustrates the phase conjugation of this kind of DFWM. In general, the signal depends also on the relative polarization of the initial waves.

The model for the DFWM in absorbing, homogeneously broadened two-level media has been worked out by Abrams and Lind [7, 8]. The Abrams–Lind (AL) model assumes undepleted pump beams ($I_f$ and $I_b$) and allows small absorption for the probe ($I_p$) and signal ($I_s$) beams. Furthermore, assumptions of monochromatic laser fields with equal pump beam intensities ($I_f = I_b = I$) and of a low $I_p$ ($I_p \ll I$) yield the laser-frequency-dependent signal intensity $I_s$:

$$I_S = RI_p = \left| \frac{\beta \sin(\gamma L)}{\gamma \cos(\gamma L) + \alpha \sin(\gamma L)} \right|^2 I_p. \qquad (3)$$

In equation (3), $R$ is defined as the phase-conjugate reflectivity; $\alpha$ is the absorption coefficient

$$\alpha = \alpha_0 \frac{1}{1+\delta^2} \frac{1 + 2I/I_{sat}}{(1 + 4I/I_{sat})^{3/2}} \qquad (4)$$

where $\delta$ is the laser detuning from the atomic transition frequency $\omega_0$, normalized with respect to the atomic transition linewidth. $\beta$ is the nonlinear coupling coefficient

$$\beta = \alpha_0 \frac{\mathrm{i} + \delta}{1+\delta^2} \frac{2I/I_{sat}}{(1 + 4I/I_{sat})^{3/2}} \qquad (5)$$

and $\gamma^2 = |\beta^2| - \alpha^2$. $\alpha_0$ is the unperturbed absorption coefficient at the line centre:

$$\alpha_0 = \frac{\omega_0 T_2}{2ch\varepsilon_0} \Delta N_0 \mu^2 \qquad (6)$$

where $\Delta N_0$ is the population difference between levels of the atomic transition in the absence of laser fields, $\mu$ is the transition dipole moment and $\varepsilon_0$ stands for the vacuum permittivity. $I_{sat}$ is the saturation intensity:

$$I_{sat} = [\varepsilon_0 ch^2/(2T_1 T_2 \mu^2)](1+\delta^2) = I_{sat}^0(1+\delta^2) \qquad (7)$$

where $T_1$ and $T_2$ are the population and coherence decay times, respectively.

In the limit of small absorption of the probe and signal beams ($\gamma L, \alpha_0 L \ll 1$), equation (3) can be simplified to the following form:

$$I_s = |\beta L^2| I_p = \alpha_0^2 L^2 \frac{1}{1+\delta^2} \frac{4(I/I_{sat})^2}{(1+4I/I_{sat})^3} I_p. \qquad (8)$$

From equation (8) it can be seen that the DFWM signal depends on the square of $\alpha_0$ and thus on the square of the unperturbed population difference $\Delta N_0$. Asymptotic forms of relation (8) in the low- and high-laser-intensity limits are given by

$$I_s \propto \alpha_0^2 L^2 \frac{1}{(1+\delta^2)^3} \frac{1^3}{(I_{sat}^0)^2} \propto \Delta N_0^2 L^2 \mu^8 T_1^2 T_2^4 \frac{I^3}{(1+\delta^2)^3} \qquad I \ll I_{sat} \qquad (9)$$

$$I_s \propto \alpha_0^2 L^2 I_{sat}^0 \propto \Delta N_0^2 L^2 \mu^2 \frac{T_2}{T_1} \qquad I \gg I_{sat}. \qquad (10)$$

At the low-intensity limit, the signal line shape $I_s$ is proportional to the Lorentzian profile of an atomic spectral line in the third power and the signal scales like the third power of the laser intensity. For the strong-intensity (saturation) regime, the DFWM signal is insensitive to the laser intensity.

The latter case can be viewed as very useful for direct monitoring of a population difference in the medium. Furthermore, when the lower level is a ground level, the DFWM signal is practically proportional to the total concentration of the probed species.

## 3. Argon arc plasma diagnostics using DFWM

A local thermal equilibrium (LTE) plasma model can be used to describe a near axis zone of an electric argon arc plasma column correctly [9–13]. It assumes a Maxwellian velocity distribution with the same temperature $T_e$ for all plasma components. The populations of atomic and ionic excited states are described by the Boltzmann distribution while the Saha equation describes the density of different plasma elements in two consecutive ionization stages. In the frame of the LTE model, the population difference $\Delta N_0$ between any two atomic states in the plasma can be calculated at given plasma temperature $T_e$ and pressure $p$ and, for a singly ionized plasma, is given by

$$\Delta N_0 = \frac{N_e^2}{S_0} \left[ \exp\left(-\frac{E_1}{k_B T_e}\right) - \exp\left(-\frac{E_2}{k_B T_e}\right) \right] \qquad (11)$$

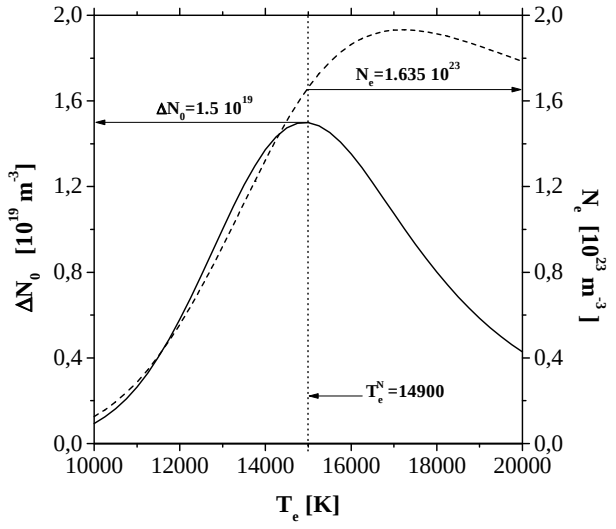


**Figure 2.** The population difference $\Delta N_0$ (full curve) between the argon states $4s[3/2]^0$–$4p'[1/2]$ and the electron density $N_e$ (broken curve) versus the plasma temperature $T_e$ calculated under LTE atmospheric pressure plasma conditions. The norm value, $\Delta N_0^N$, corresponds to $1.506 \times 10^{19}$ m$^{-3}$ at the norm temperature $T_e^N$ = 14 900 K.

where $N_e$ is the free electron density, $E_1$ and $E_2$ are the energies of the lower and upper states, $k_B$ is the Boltzmann constant and $S_0 = S_0(T_e)$ is the Saha function for this atomic component [11, 12].

We define the norm population difference $\Delta N_0^N$ as the maximum value of $\Delta N_0$ attainable at the specific temperature $T_e^N$ (called the norm temperature) for the LTE atmospheric pressure plasma. These terms are introduced in a similar way to the norm intensity and temperature for spectral lines [11]. The population difference $\Delta N_0$ between two specific argon states ($4s[3/2]^0$ and $4p'[1/2]$, for the 696.5 nm ArI line), calculated for the LTE atmospheric pressure plasma, versus the plasma temperature is plotted in figure 2 with the full line. The norm population difference and the appropriate norm temperature have values of $1.506 \times 10^{19}$ m$^{-3}$ and 14 900 K, respectively, and are marked in figure 2. For the sake of completeness, the temperature dependence of the free electron density (under the LTE plasma model) is also plotted in figure 2 with the broken curve. Once the norm temperature has been reached and $\Delta N_0^N$ measured at some place in the investigated plasma volume, $\Delta N_0$ can be derived at any plasma position, $x$, from the relation

$$\Delta N_0(x) = \Delta N_0^N [I_s(x)/I_s(N)]^{1/2} \qquad (12)$$

where $I_s(x)$ and $I_s(N)$ are the DFWM signals measured at the position $x$ and at the position of the maximum (norm value) $\Delta N_0^N$, respectively. The plasma temperature and electron density can subsequently be calculated using the LTE plasma equation set [11].

The AL theory of the DFWM in its high-laser-intensity limit gives the simple formula equation (10), which is especially useful in the case of the LTE plasma. The signal's sensitivity to the relative dephasing rate $(T_2/T_1)$ is greatly reduced as a result of the domination of electron collision processes in the plasma, where both $T_1$ and $T_2$ are directly proportional to the electron density, so their ratio has a constant value throughout the studied plasma volume.

In all applications of the DFWM, special attention should be paid to the problem of atomic motion, which was neglected in the AL theory. The assumption of a homogeneously broadened line is well satisfied in our case when we compare the homogeneous Stark width of 277 GHz (calculated for the norm temperature) with the 22 GHz Doppler width. On the other hand, significant 'washout' of the grating can occur, resulting in signal attenuation. This effect appears when an atom travels a great part of the grating period $\Lambda$ (equation (1)) during the grating lifetime defined by the population decay time $T_1$. Such an effect of the atomic motion on the DFWM was studied by Wandzura [14]. He introduced a DFWM signal attenuation parameter $m(\Gamma, \theta)$, where $\Gamma$ is the ratio of the grating's lifetime to an atom's mean velocity and $\theta$ is the angle between the probe and pump laser beams (see figure 1). Under our LTE plasma conditions, the calculated attenuation parameter changes from 0.607 to 0.569 in the temperature range 12 000–20 000 K and can be neglected. From the above discussion we conclude that the DFWM signal variation in our homogeneous plasma volume is predominantly due to the variation in the population difference $\Delta N_0$, enhanced by the quadratic dependence in equations (9) and (10).

## 4. The experimental set-up

The experimental arrangement is shown in figure 3. It consisted of the studied plasma source, the laser and the detection system. The plasma source has been described in detail in [15]. Briefly, the arc discharge was generated from a conical tungsten cathode tip ($\alpha = 40^\circ$ conical angle) of 4 mm diameter and surrounded by a water-cooled nozzle. In its upper part, the arc consisted of three copper discs with a 5 mm channel in the centre. The third disc served as the anode. The arc was operated in pure argon and its flow of 2.0 l min$^{-1}$ was maintained. The arc was powered by current in the range 70–120 A.

A tunable dye laser ($\lambda$ near 696.54 nm) was pumped by the second harmonic of a Nd:YAG laser with a 5 Hz repetition rate. The dye laser was operated with Oxazine 725 and provided 10 ns pulses of about 600 $\mu$J energy with a spectral bandwidth less than 9 GHz. The output beam of the dye laser was split into a forwards-pump beam $I_f$ and a probe beam $I_p$ with an intensity ratio of 8:1. The forwards beam was reflected from a dielectric concave mirror M1 back into the plasma interaction region and acted as a third, backwards-pump beam $I_b$. The 500 mm focal length lenses (L1 and L2) and the 200 mm focal length mirror (M1) were used to focus the laser beams at the plasma symmetry axis with a waist diameter smaller than 0.1 mm. In the phase-conjugate geometry of figure 1, two counter-propagating pump beams crossed with the probe beam at an angle of about 14°, which determined the spatial resolution of the method to be 0.1 mm longitudinally and 0.35 mm transversally with respect to the laser beam. In our experiment we employed a crossed polarization

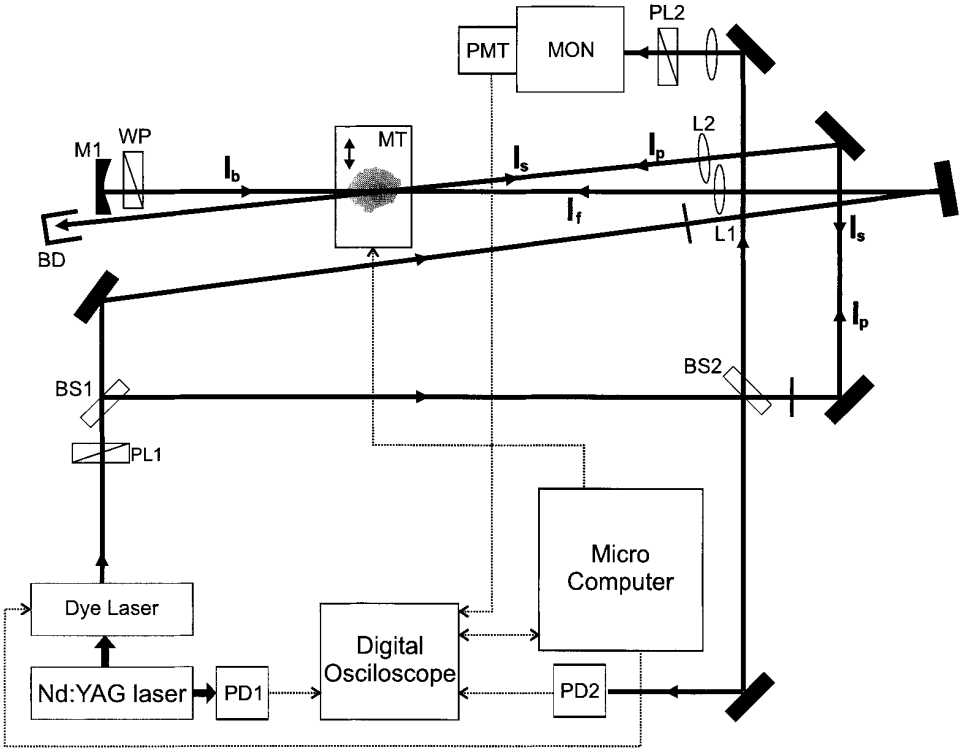


**Figure 3.** The experimental arrangement: PD1 and PD2, photodiodes; PL1 and PL2, polarizers; BS1 and BS2, beam splitters; L1 and L2, lenses; M1, concave mirror; WP, quarter-wave plate; and PMT, photomultiplier.

configuration in which a quarter-wave plate (WP) was used in order to rotate the polarization of the backwards-pump beam 90° with respect to that of the horizontally polarized forwards-pump and probe beams.

The generated DFWM signal $I_s$ propagated backwards along a probe beam path, was reflected from the plate BS2 and was directed towards the detection system. The DFWM signal had the same polarization as the backwards-pump beam, which allowed polarizer PL2 to reject the probe-beam light scattered from the beam splitters and other optical elements efficiently. This probe-beam-scattered light appeared to be the dominant source of the background noise. The signal detection was performed by using a fast photomultiplier (Hamamatsu R928) installed behind the exit slit of a monochromator. The PMT signal was then directly connected to a digital oscilloscope (300 MHz bandwidth), externally triggered by the Nd:YAG laser pump light pulses. The dye laser intensity was monitored by a PD2 photodiode connected to the second channel of the scope. Signals were averaged over 20–50 laser shots and then integrated over a time period of 60 ns.

The radial and horizontal profiles of the DFWM signal were obtained by translation of the plasma arc with a step-motor drive. The whole acquisition system was operated and controlled by a computer.

## 5. Results and discussion

Figure 4 presents the DFWM signal versus the laser intensity obtained for the argon plasma discharge operated at 90 A and measured on the plasma's symmetry axis ($R = 0$ mm), 1 mm above the cathode tip. The full curve is a theoretical fit to experimental data according to equation (7). Figure 4 shows that we reached the saturation limit and the AL theory correctly described our signals.

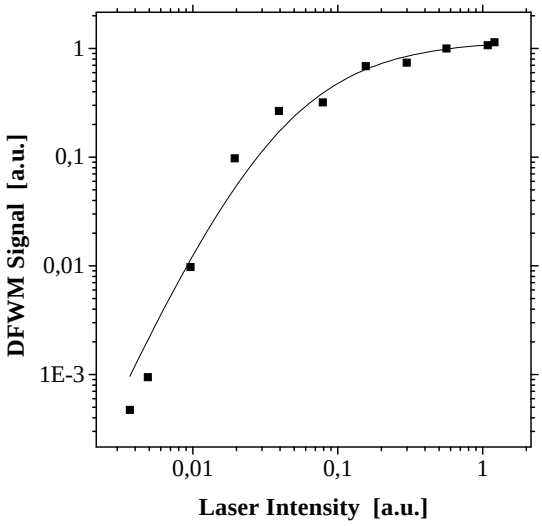


**Figure 4.** A comparison of the experimental (■) and theoretical (——) DFWM signal dependences on the laser intensity. The theoretical curve was calculated according to the AL theory (equation (8)) for the resonance excitation ($\delta = 0$).

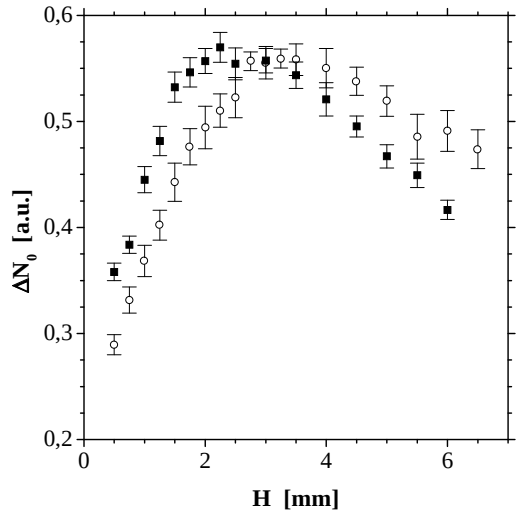


**Figure 5.** The axial distribution of the population difference $\Delta N_0$ ($H$ = 0 mm corresponds to the cathode tip), obtained from the DFWM signals measured in the high-laser-intensity limit: (■), 120 A; and (○), 70 A plasma arc current.

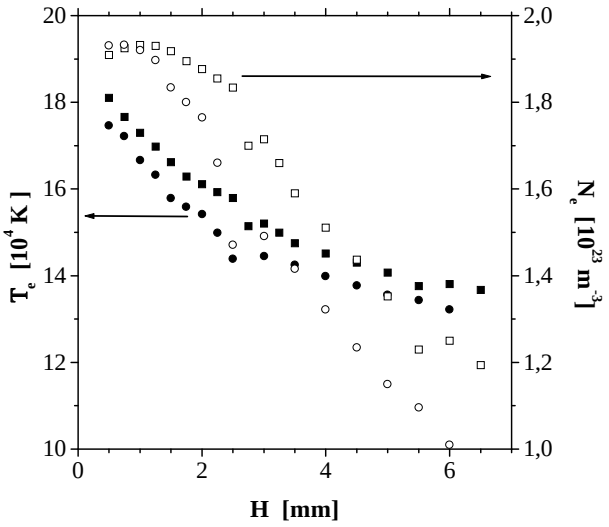


**Figure 6.** Axial distributions of the plasma temperature (full symbols) and electron density (open symbols), determined from the DFWM signals as described in section 3: (●,○), 70 A; and (■,□), 120 A plasma arc current.

The population difference $\Delta N_0$, according to equation (10) is derived as the square root of the DFWM signal. Its axial variations, for the plasma operated at 'low' (70 A) and 'high' (120 A) currents, are shown in figure 5. In both cases, $\Delta N_0$ exhibited a maximum, at distance of 2.35 and 3.6 mm above the cathode for the low- and high-current cases, respectively.

From our previous OES measurements [13], we know that, for this plasma source, the temperature on the arc axis grows towards the cathode and the LTE state exists in the near-axis plasma zone. Therefore, from figure 5, we conclude that the axial maximum of $\Delta N_0$ corresponds to the norm value defined in section 3, with the norm temperature $T_e^N = 14\,900$ K and free electron density $N_e = 1.635 \times 10^{23}$ m$^{-3}$.

The axial temperature and electron density distributions were determined as described in section 3 and are shown in figure 6. The full and open symbols stand for the plasma temperature and electron density while circles and squares are for low and high arc currents, respectively. Figure 6 displays an axial temperature increase in the cathode direction. For the higher current the temperature remains about 500 K higher than that for the lower one, all along the plasma axis.

Unlike the temperature, close to the electrode (within 1.25 mm), the electron density exhibited its maximum value under the LTE atmospheric plasma conditions (see figure 2) and exhibited no variation with a further approach towards the electrode. On the other hand, above 1.5 mm separation, $N_e$ rapidly decreased with the distance from the electrode.

Under the same plasma conditions, radial (perpendicularly to the plasma axis) DFWM measurements were performed and their results are summarized in figure 7. The first, second and third columns are the population difference, plasma temperature and electron density, respectively, taken at axial positions $H = 0.5$, 2.0 and 4.0 mm above the cathode's tip. There was an evident shift of the plasma axis for the two different currents used. It may have been caused by migration of the cathode spot on the cathode surface when the plasma current was switched from one value to another and it was more pronounced close to the cathode. Figure 7 shows that, for high current, $\Delta N_0$ has the same maximum value for $H = 4.0$ mm (axis maximum) and $H = 2.0$ mm (off-axis maximum), equal to the norm value. However, for $H = 0.5$ mm the off-axis maximum had a smaller value, which contradicts the LTE atmospheric pressure plasma model. This effect had already been observed for the 696.5 nm ArI line in OES and explained by Pokrzywka *et al* [15] and by Haidar [16]. In the low-current case, the measured signal was close to the norm population difference only for $H = 2.0$ mm whereas for $H = 4.0$ mm, $\Delta N_0$ was lower than the norm value all along the plasma radius. For $H = 0.5$ mm, the off-axis maximum of $\Delta N_0$ was lower than the norm value for the same reason as for the high-current case.

The radial temperature and electron density distributions determined from $\Delta N_0$ are presented in columns 2 and 3 of figure 7. The plasma temperature displayed a very well defined maximum placed on the plasma axis which changed from 17 200 to 14 800 K and from 16 200 to 14 000 K for the high- and low-current plasmas, respectively. Its radial distribution exhibited steeper gradients close to the electrode ($H = 0.5$ mm) and in the range of 2 mm from the axis the temperature could decrease by as much as 5000 K.

A similar dependence was obtained for the electron density distribution with a little difference near the cathode where a distribution plateau extends over 2 mm diameter ($H = 0.5$ mm and high-current plasma). Its maximum radial value changed only from $1.93 \times 10^{23}$ m$^{-3}$ ($H = 0.5$ mm, high-current case) to $1.5 \times 10^{23}$ m$^{-3}$ ($H = 4.0$ mm) but steep radial variations were its main feature. Near the electrode the electron density dropped by a factor of four on moving only 2 mm away from the arc axis.

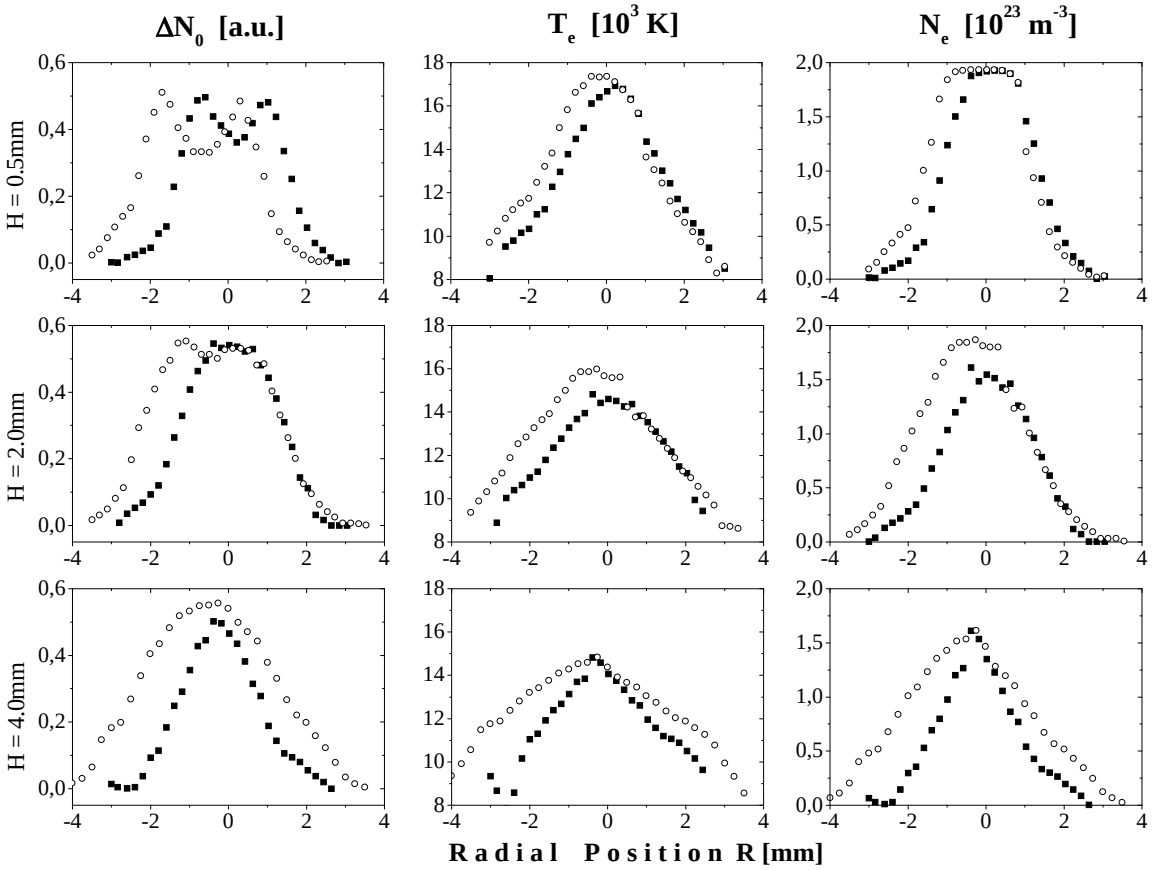


**Figure 7.** Radial distributions of the population difference $\Delta N_0$, the plasma temperature $T_e$ and the electron density $N_e$ determined at different axial positions $H$ = 0.5, 2.0 and 4.0 mm above the cathode tip: (■), 70 A; and (○), 120 A plasma arc current.

Owing to the drop in the electron density and the near-cathode-zone phenomena described in [15], the LTE plasma assumption must be validated in these regions. When we follow a criterion for the LTE state in the argon plasma, $N_e > 5 \times 10^{22}$ m$^{-3}$ given in [17], the assumption for the LTE is satisfied for a long axial distance but it already breaks down 1.5 mm away from the plasma axis. Therefore, beyond this region (the near-axis zone), our results should be corrected for the imperfection of the LTE state in the plasma. A discussion of the equilibrium state for this plasma source can be found in [15].

## 6. Conclusions

The non-intrusive DFWM method was used to study the LTE atmospheric pressure argon arc plasma. The laser wavelength was in resonance with the $4s[3/2]^0$–$4p'[1/2]$ ArI transition, corresponding to the 696.5 nm line. The Abrams–Lind theory was verified and proved to be valid by application to our plasma. DFWM signals were shown, in the high-laser-intensity limit, to be exclusively dependent on the population difference between the involved argon states. Well resolved axial and radial profiles of plasma temperature and electron density were determined. The occurrence of a deviation from the LTE plasma model near the cathode tip, despite the high plasma temperature and the electron density, was confirmed.

The main advantages of the DFWM are due to its relatively simple and fast data processing; the sampling of a small, uniform plasma volume; the direct proportionality of the measured signal to the atomic transition population difference $\Delta N_0$ and its reasonably high spatial resolution. Useful information, such as the local component concentrations, plasma temperature and electron density, may be obtained for asymmetrical plasmas. Furthermore, two-dimensional diagnostics of the entire plasma can be performed with one laser shot when a sufficiently intense laser and a diode-matrix detector are used.

In addition to the above application, the measurement of the Stark broadening and spectral line shifts in the LTE plasma regions could be another attractive application of the DFWM. It would combine both the low- and the high-laser-intensity limit of the AL theory. The first one would give a measured line profile, narrower than the corresponding emission line, whereas the second would allow determinations of the plasma temperature and electron density.

## Acknowledgment

This research was supported by the Polish Committee for Scientific Research, grant 2P30205205.

## References


[1] Ewart P, Snowdon P and Magnusson I 1989 *Opt. Lett.* **14** 563
[2] Farrow R L, Rakestraw D J and Dreier T 1992 *J. Opt. Soc. Am.* B **9** 1770
[3] Dreier T and Rakestraw D J 1990 *Appl. Phys.* B **50** 479
[4] Williams S, Green D S, Sethuraman S and Zare R N 1992 *J. Am. Chem. Soc.* **114** 9122
[5] Nyholm K, Kairola M and Aminoff C G 1994 *Opt. Commun.* **107** 406
[6] Georgiev N and Alden M 1993 *Appl. Phys.* B **56** 281
[7] Abrams R L and Lind R C 1978 *Opt. Lett.* **2** 94
[8] Abrams R L, Lam J F, Lind R C, Steel D G and Liao P F 1983 Phase conjugation and high resolution spectroscopy by resonant four wave mixing *Optical Phase Conjugation* ed R A Fisher (New York: Academic) p 240
[9] Shumacker J B and Popenoe C M 1972 *J. Res. NBS* A **76** 305
[10] Nubbemeyer H 1976 *J. Quant. Spectrosc. Radiat. Transfer.* **16** 71
[11] Neumann W 1975 Spectroscopic methods of plasma diagnostics *Progress in Plasmas Gas Discharges* ed R Rompe and M Steenbeck (Berlin: Akademie) p 95
[12] Griem H R 1964 *Plasma Spectroscopy* (New York: McGraw Hill) p 179
[13] Pellerin S, Musioł K, Pokrzywka B and Chapelle J 1994 *J. Phys. D: Appl. Phys.* **27** 522
[14] Wandzura S M 1979 *Opt. Lett.* **4** 208
[15] Pokrzywka B, Musioł K, Pellerin S, Pawelec E and Chapelle J 1996 *J. Phys. D: Appl. Phys.* **29** 2644
[16] Haidar J 1995 *J. Phys. D: Appl. Phys.* **28** 2494
[17] Nick K P, Richter J and Helbig V 1984 *J. Quant. Spectrosc. Radiat. Transfer* **32** 1